

NUMERICAL SIMULATION OF A CUBICAL CAVITY FILLED WITH OIL SHOWING TEMPERATURE-DEPENDENT VISCOSITY

Paola A. Córdoba^a, Nicolás Silin^{b,c} and Enzo A. Dari^{a,c}

^a*Departamento de Mecánica Computacional, Centro Atómico Bariloche-CNEA, Instituto Balseiro-UNCU, CONICET, Av. Bustillo 9500, S.C. de Bariloche, Río Negro, Argentina, paolaco@cab.cnea.gov.ar*

^b*Grupo de Materiales Nucleares, Centro Atómico Bariloche-CNEA, Instituto Balseiro-UNCU, CONICET, Av. Bustillo 9500, S.C. de Bariloche, Río Negro, Argentina, silin@cab.cnea.gov.ar*

^c*Member of CONICET, Argentina*

Keywords: Natural convection, Cubical Cavity, temperature-dependent viscosity, Finite Element Method.

Abstract. We performed a numerical and experimental study of laminar natural convection flow in an oil filled cubical cavity. The fluid is a dielectric oil used for cooling distribution and power transformers. This fluid has temperature-dependent viscosity. The cubical cavity of interest has an imposed temperature difference between two opposite vertical walls while the other walls are insulated. The cavity dimensions are 0.1m x 0.1m x 0.1m were a flow with a characteristic Rayleigh number $Ra = 1.7 \times 10^8$ was obtained. The numerical study was carried out by applying the Finite Element Method to solve the 3D Navier-Stokes and heat equations using the in-house developed Par-GPFEP code. The influence of the temperature viscosity dependence on total heat transferred and the flow pattern have been evaluated. An experimental setup was developed to validate the numerical results. The temperature profiles in the vertical mid-axis at mid-plane of the cavity were measured and compared with the numerical results. We found reasonable agreement between numerical simulations and experimental measurements. Although there are several studies of the flow in a square cavity in this configuration, there is limited information in the literature regarding 3D flow in cubical cavities with variable properties of the working fluid. This work provides numerical and experimental data in this wide unexplored problem that can be used as benchmark to validate CFD models as well as to understand how to optimize devices based on natural convection cooling processes.

1 INTRODUCTION

The problem of natural convection flow in a cubical cavity with two opposite side walls differentially heated and the remaining four walls adiabatic (from now on we will call this configuration CC) is a benchmark frequently used to validate CFD codes not only for the geometry simplicity but also for their engineering interest. Thermal engineering applications range from double glazed windows, solar collectors, cooling of thermal-hydraulic devices, among others (Buchberg et al., 1976; Gastelurrutia et al., 2011).

Several studies regarding the square cavities can be found in the literature, these cover a wide range of Rayleigh (Ra) numbers ranging from 10^3 to 10^{16} . The first benchmark of the square cavity was reported by De Vahl Davis (1983), who presented flow results at steady state in a square cavity at a Prandtl (Pr) number $Pr = 0.71$ and Rayleigh numbers from 10^3 to 10^6 . A large number of authors have extended this range using different experimental and numerical techniques. Much of the work related to the square cavity has been referenced by Arpino et al. (2010) who proposed a new square cavity benchmark solution at $Ra = 10^7$ to 10^8 , his results were validated with numerical and experimental results from other authors.

In contrast, the flow in cubical cavities have been less studied. On the one hand the computational cost becomes more elevated with increasing Rayleigh number and on the other hand, there are considerably few experimental studies to validate the numerical results. One of the first experimental works is the research of Hiller et al. (1989) on a cubical cavity that was filled with a glycerol-water solution over a Rayleigh number range from 10^4 to 10^7 . They observed the temperature fields and flow streamlines and found discrepancies with numerical results from other authors. The authors attribute these differences to the fact that the numerical model did not consider temperature dependent viscosity. Recent studies are the experimental works of Leong et al. (1998b), Leong et al. (1998a) and Mamun et al. (2003). They studied the cubical cavity in a different configuration: a cubical cavity with two opposite walls heated at different temperatures, the remaining faces with a lineal variation of the cold temperature to the hot temperature. They also studied the effect of the tilt angle of the cavity respect to the gravity force.

They remark the fact that the other configurations like the CC benchmark are not physically-realizable. The sense of this affirmation is that in an air-filled cavity the heat losses at the walls are especially critical due to the low thermal conductivity of the air.

With regard to numerical studies, the first one, was the work of Mallinson and Davis (1977). They studied the three-dimensional flow in a box, varying the cavity dimensions, the Rayleigh and Pr numbers. They analyzed how the three-dimensionality of the flow is affected by these three parameters. Most of the numerical studies focus on the air-filled cubical cavity, considering constant properties and Rayleigh numbers ranging from 10^3 to 10^7 . Some examples are the works of Fusegi et al. (1991), Tric et al. (2000), Wakashima and Saitoh (2004), Peng et al. (2004), Bennett and Hsueh (2006). They used this benchmark (CC) to validate different numerical techniques. Pepper and Hollands (2002) made a summary of several numerical studies of three benchmark problems, one of them is the air-filled enclosure proposed by Leong et al. (1998b), in a range of Rayleigh numbers from 10^5 to 10^8 . This new configuration is convenient from both the experimental and numerical point of view. Not only for its experimental feasibility but also as it becomes unstable at lower Ra numbers. This allows to perform numerical solutions without the need of a high spatial definition (Janssen et al., 1993).

In this work we present a Numerical and experimental study of laminar natural convection in the CC benchmark problem. The fluid is a dielectric oil used for cooling electrical equipment, specifically the YPF64 oil which is frequently used in distribution transformers using ONAN

(oil-natural, air-natural) heat transfer management scheme. This mineral oil type has a strong viscosity variation in the working range of temperatures. The main objective is the observation and quantification of variable viscosity effects in flow pattern and heat transfer rate in CC configuration. We studied the flow at Rayleigh number 1.7×10^8 and no turbulent model was used since the transition to turbulence begins between 10^8 to 10^9 (Chenoweth and Paolucci, 1986; Paolucci and Chenoweth, 1989) and numerical and experimental results showed a laminar flow.

2 MATHEMATICAL MODEL

2.1 Geometry and General Aspects

We consider a cubical enclosure with height, width and depth L as is illustrated in Fig. 1. The left and right vertical walls are both isothermal with temperature T_c and T_h ($T_h > T_c$) respectively. The remaining four walls are thermally insulated. YPF64 oil with temperature-dependent viscosity is the working fluid. The physical properties of this mineral oil are shown in Table 1.

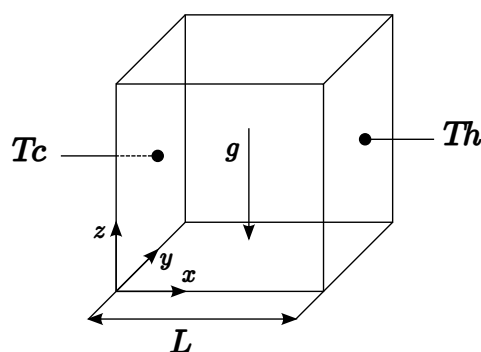


Figure 1: Geometrical description of the cavity and coordinates system.

Physical property	Value	
Density (kg/m ³)	ρ	880
Thermal conductivity (W/mK)	k	0.126
Specific Heat (J/kgK)	C_p	1860
Thermal expansion coefficient (K ⁻¹)	β	0.00075

Table 1: Fluid properties of the YPF64 oil.

2.2 Governing Equations

The cubical cavity flow is governed by the incompressible Navier-Stokes, and Energy equations, where the Boussinesq approximation is considered. The dimensional form of this equations can be expressed in cartesian coordinates as

$$\rho_0[\partial_t u + (u \cdot \nabla)u] - \nabla \cdot [2\mu(T)\nabla^s u] + \nabla p = f \quad \text{in } \Omega, \quad t \in (0, T), \quad (1)$$

$$\nabla \cdot u = 0 \quad \text{in } \Omega, \quad t \in (0, T), \quad (2)$$

$$\rho_0 C_p[\partial_t T + (u \cdot \nabla)T] - k\nabla^2 T = 0 \quad \text{in } \Omega, \quad t \in (0, T), \quad (3)$$

where u is the velocity vector with components u_x , u_y and u_z , $f = \rho_0 g[1 - \beta(T - T_0)]$ is the buoyancy force, $\nabla^s u = \frac{1}{2}[(\nabla u) + (\nabla u)^T]$ is the symmetric gradient operator. Ω is the N_{sd} -dimensional domain where the problem will be solved in the time interval $(0, T)$. We use the no-slip boundary conditions for velocity at all walls,

$$u_x = u_y = u_z = 0 \quad \text{at} \quad \begin{cases} x = 0, & L, \\ y = 0, & L, \\ z = 0, & L. \end{cases} \quad (4)$$

For the energy equation, the left and right vertical walls have Dirichlet boundary conditions (5) and the other four walls have Neumann conditions (6).

$$\begin{aligned} T &= T_h \quad \text{at} \quad x = L, \\ T &= T_c \quad \text{at} \quad x = 0, \end{aligned} \quad (5)$$

$$\begin{aligned} \frac{\partial T}{\partial y} &= 0 \quad \text{at} \quad y = 0, L, \\ \frac{\partial T}{\partial z} &= 0 \quad \text{at} \quad z = 0, L. \end{aligned} \quad (6)$$

As initial condition we take constant quantities for velocity, pressure and temperature to obtain a numerical solution in a coarse mesh. This solution is used as initial condition by interpolating in finer grids.

2.3 Solution Method

The equations (1)-(3) have been solved by the Finite Element Method. In this work we use the Standard Galerkin approximation with the addition of stabilizer terms according to the SUPG method (see Codina (1998)). With this technique, the variational formulation of problem (1)-(3) consists in finding finite element approximations $(u_h^{n+\theta}, p_h^{n+1}, T_h^{n+\theta})$ to $(u^{n+\theta}, p^{n+1}, T^{n+\theta})$ such that

$$\begin{aligned} \rho_0 \left(\frac{u_h^{n+1} - u_h^n}{\Delta t} + (u_h^n \cdot \nabla)u_h^{n+\theta}, v_h \right) + 2\mu(T_h^n) \cdot a(u_h^{n+\theta}, v_h) - b(p_h^{n+1}, v_h) - (f^n, v_h) + \\ \sum_{e=1}^{nel} \int_{\Omega^e} \left(\mathcal{P}(u_h, v_h) \tau \mathcal{R}(u_h, p_h) + (4\mu + 2\rho_0 \|u^n\| h_e) \nabla \cdot u_h^{n+1} \nabla \cdot v_h \right) d\Omega = 0 \quad \forall v_h \in V_{h,0}, \end{aligned} \quad (7)$$

$$b(q_h, u_h^{n+1}) + \sum_{e=1}^{nel} \int_{\Omega^e} \tau \mathcal{R}(u_h, p_h) \cdot \nabla q_h d\Omega = 0 \quad \forall q_h \in Q_h, \quad (8)$$

$$\begin{aligned} & \left(\frac{T_h^{n+1} - T_h^n}{\Delta t} + (u_h^n \cdot \nabla) T_h^{n+\theta}, w_h \right) + \alpha \cdot a(T_h^{n+\theta}, w_h) \\ & + \sum_{e=1}^{nel} \int_{\Omega^e} \mathcal{P}(u_h, w_h) \tau_1 (u_h^n \cdot \nabla) T_h^{n+\theta} d\Omega = 0 \quad \forall w_h \in W_h, \end{aligned} \tag{9}$$

with the finite element spaces $Q_h, V_h, V_{h,0}$ and W_h which are approximations to $Q_{st} = \{q \in L^2(\Omega) | \int_{\Omega} q = 0\}$, $H^1(\Omega)^{Nsd}$, $V_{st} = H_0^1(\Omega)^{Nsd}$ and $W_{st} = H_D^1(\Omega)^{Nsd}$ respectively with the following bilinear forms:

$$\begin{aligned} a(u_h^{n+\theta}, v_h) & := (\nabla^s u_h^{n+\theta}, \nabla^s v_h), \\ b(q_h, u_h^{n+1}) & := (q_h, \nabla \cdot u_h^{n+1}), \end{aligned} \tag{10}$$

the perturbation to the test function \mathcal{P} of the form:

$$\mathcal{P}(u_h, v_h) = (u_h \cdot \nabla) v_h, \tag{11}$$

and \mathcal{R} the residual of the momentum equation

$$\mathcal{R}(u_h, p_h) = \rho_0 \left[\frac{u_h^{n+1} - u_h^n}{\Delta t} + (u_h^n \cdot \nabla) u_h^{n+\theta} \right] + \nabla p_h^{n+1} - f^n, \tag{12}$$

τ is the intrinsic time that depends of the stabilizing technique, we use the definition of [Codina \(1998\)](#) for momentum and energy equations respectively, written as follows,

$$\tau = \frac{1}{\frac{4\mu}{\rho_0 h_e^2} + \frac{2\|u\|}{h_e}} \quad \tau_1 = \frac{1}{\frac{4\alpha}{h_e^2} + \frac{2\|u\|}{h_e}}, \tag{13}$$

where h_e is the element size in the flow direction. For the temporal discretization we use the trapezoidal rule scheme:

$$u^{n+\theta} := \theta u^{n+1} + (1 - \theta) u^n. \tag{14}$$

In this work we use $\theta = 1/2$ (Crank-Nicolson) for the momentum equation and $\theta = 1$ (Backward Euler) for the energy equation. A detailed discussion about this scheme can be found in [Codina \(1992\)](#). The resulting system of linear equations was solved by the iterative method GMRES with a block-ILU preconditioner which is implemented in the in-house developed Par-GPFEP code ([Lew, 1998](#)).

2.4 Temperature dependence viscosity

Due to the limited technical specifications available for this mineral oil, the dependence of viscosity with temperature was experimentally measured with a Brookfield DV-II+ Pro programmable cone/plate viscometer. To provide a controlled variation of temperature a HAAKE D8 temperature bath controller coupled to the viscometer was used. The viscosity measurements are shown in Fig. 2.

This figure shows the experimental data and its fitting function in logarithmic scale. We found that the viscosity of the working oil can be fitted with the following law:

$$\log(\mu(T)) = B - A \log(T), \tag{15}$$

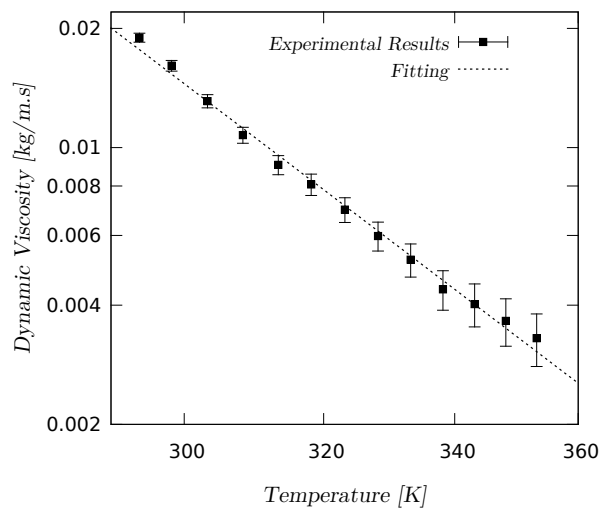


Figure 2: Characteristic curve of the viscosity as a function of temperature for mineral oil YPF64 in logarithmic scale.

where $A = 9.55 \pm 0.23$, $B = 50.24 \pm 1.33$, μ is expressed in kg/ms and temperature T in Kelvin scale. This potential law was implemented in the solver code to account for viscosity variations with temperature. In the case studied in the present work, the wall temperatures T_h and T_c were set to 50°C and 30°C respectively. The difference of temperatures was 20°C giving a Rayleigh number of 1.7×10^8 with oil material parameters evaluated at the film temperature $T_f = (T_h + T_c)/2$. Notice that for this wall temperatures, the dynamic viscosity varies from ~ 0.007 to ~ 0.013 kg/ms, resulting in a difference with respect to the mean value, of $\sim 60\%$.

2.5 Characteristic scales and Grid Size

In order to determine the grid size, a first estimation of the thickness of the thermal and momentum boundary layers (δ_θ , δ) were made using the expression (16) in terms of a dimensionless number Π_N , introduced by Arpaci (1986), which represents the heat transfer by natural convection for a wide range of Pr number.

$$\frac{\delta_\theta}{l} \sim \Pi_N^{-1/4}, \quad (16)$$

$$\Pi_N = \frac{Pr}{1 + Pr} Ra, \quad (17)$$

with the assumption of $\delta_\theta \sim \delta$. In our case, with a $Ra = 1.7 \times 10^8$ and $Pr = 142$, the value of δ_θ is about $\sim 9 \times 10^{-4}$ m. Taking into account the thickness of the boundary layer, three non-uniform structured grids were built and used in order to make a grid independency study. The Table 2 shows the minimal spatial discretization h_{min} and also, the dependence of total heat transfer with the grid size. It can be noted that the difference between C and M is about 3.4% whereas the difference between M and F is much lower, about 0.07%.

This behavior is also presented in the pattern of the flow as is plotted in Fig. 3 which presents the vertical profiles of temperature and velocity at mid-plane of the cavity for the three mesh sizes. The velocity is presented in a dimensionless form by using the velocity characteristic length $U_0 = \sqrt{g\beta L(T_h - T_c)}$. It can be concluded that the results obtained with the meshes M and F are practically grid independent and also can solve the boundary layers near the walls.

Mesh	Grid Size	\overline{Nu} (Hot Wall)	\overline{Nu} (Cold Wall)	h_{min} (m)
C	$50 \times 50 \times 50$	35.04	35.13	5.00×10^{-4}
M	$120 \times 120 \times 120$	36.27	35.97	2.50×10^{-4}
F	$150 \times 150 \times 150$	36.27	36.20	1.42×10^{-4}

Table 2: Grid dependence of Nusselt number in different meshes.

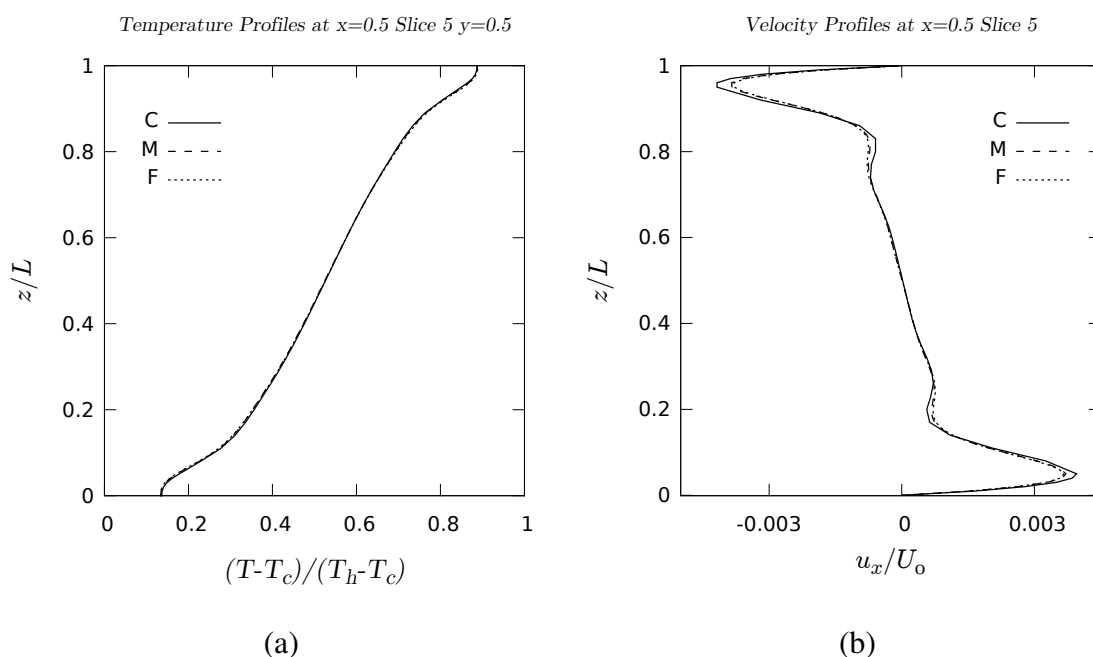


Figure 3: Grid dependence of vertical profiles at mid-plane of the cavity. (a) Temperature profile, (b) x-component of velocity profile.

3 EXPERIMENTAL SETUP AND MEASUREMENT METHOD

The experimental device is a cubical cavity completely filled with mineral oil YPF64. The cavity is formed by two vertical and opposed aluminum walls and four transparent walls. The superior wall is made of 4 mm thick crystal acrylic and the remaining three are made of window glass. The spacing between walls is 100 ± 0.5 mm. A schematic of the experimental device is shown in Fig. 4.

The upper wall has two 4 mm penetrations, one for the insertion of the traversing temperature sensor and the other for the expansion tank. The aluminum walls provide the hot and cold fixed temperature conditions. The hot wall is 24 mm thick and is heated by means of a Watlow FIREROD cartridge electrical heater, with diameter and heating length of 6.5 mm and 50 mm respectively, inserted at 18 mm from the internal surface. The temperature is controlled by a Novus N480D temperature controller in PID mode and the power is measured by averaging the applied electric voltage and using the measured resistance value of the heater. The cold wall is refrigerated by means of a glycol and water mixture flow provided by a thermostatic bath. The fluid is passed by a winding copper tube soldered to a flat slab that is in good thermal contact

with the aluminum wall. Two PT100 transducers are inserted into the hot and cold walls to measure their temperature. The traversing temperature transducer is a 0.5 mm in diameter NTC glass thermistor (GE P20 Thermoprobe). It was calibrated by means of a Techne Tecal 650S temperature calibrator giving a measurement precision of 0.5 °C. Temperature measurements were taken by a National Instruments NI 9219 universal analog input module. Voltage measurements were taken by means of a resistor divider bridge connected to a NI 9205 analog input module, both connected to a PC. The cavity was covered with expanded polystyrene of 20 mm thick and a thermal conductivity $k_{wall} = 0.038$ W/mK, to provide the thermal insulation of the cavity (see Fig. 5).

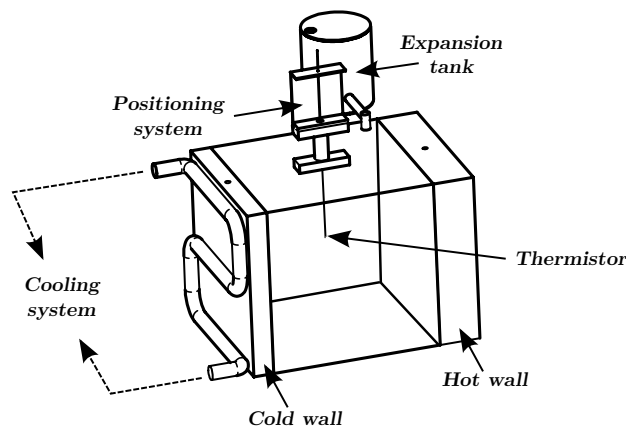


Figure 4: Schematic of the experimental device.

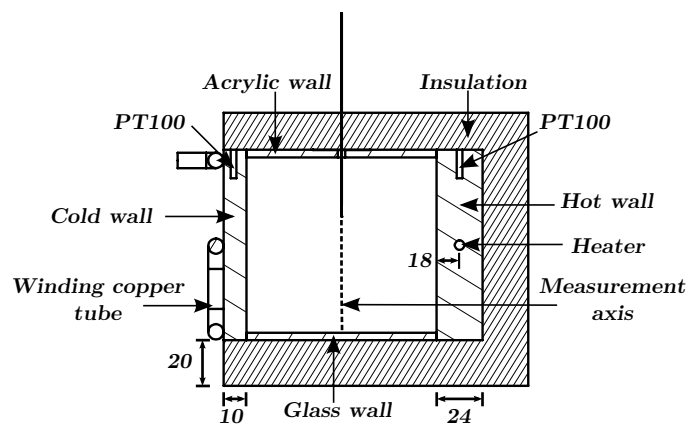


Figure 5: View of the cavity center slice with the thermal insulation, the length units are expressed in mm.

The vertical temperature profile was measured, with the thermistor moving along the z-axis at mid-width and mid-height of the cavity, once the steady state was achieved. This state was monitored by the time evolution of the temperatures in the isothermal walls and was reached when both temperatures got a stable value.

4 RESULTS AND DISCUSSION

4.1 Numerical Results

This work presents two numerical simulations in order to compare the heat transfer and the pattern of the flow between a fluid with constant and variable viscosity. The first one was performed with variable viscosity according to the potential law (15), and the second one, with constant viscosity at the film temperature T_f .

Streamlines at different vertical planes parallel to the x axis of the cavity are shown in Figs. 6 and 7. As can be noted in both cases, the streamlines on top and the bottom of the cavity bend their lines toward the center of the plane, in slices near to the front wall (window), while the curvature is less pronounced in slices closest to the mid-plane. This fact exhibits the three-dimensional character of the flow.

Furthermore, the pattern of the flow at this Rayleigh number is characterized by the presence of three vortices. One of them is the central vortex which corresponds to the main flow inside the cavity following its geometry and transporting the 90% of the mean flow rate whereas the others two vortices, verticals and adjacent to the isothermal walls, transport only the 10% of the mean flow rate, being a secondary flow. With regard to the flow pattern, the main difference found between the two cases was the aspect of the central vortex core. In the first case (variable viscosity), this elongated convective roll is asymmetric, being wider near the hot wall and narrower near the cold wall. The viscosity is smaller near the hot wall while is maximal in the cold one, this generates higher velocities and a narrower boundary layer near the hot wall. In contrast, the second case shows a symmetric convective core in central planes which is affected by boundary effects in planes nearest to the end walls. The asymmetry caused by variations in the fluid viscosity have been documented by other authors like Hyun and Lee (1988). They studied the square cavity differentially heated with a fluid having a temperature-dependent viscosity at a Rayleigh number of 3.5×10^5 in a square cavity.

The central core region velocities are lower than those near the walls, where the velocity and temperature gradients are significant (see Fig. 8a). This behavior is observed quantitatively through vertical and horizontal velocity profiles along the cavity mid axis from figure Fig. 8.

Notice that in Fig. 8a the velocity z-component in horizontal profiles are not affected by boundary effects of the end walls, contrary to the velocity x-component from vertical profiles (see Fig. 8b) where there are notable effects of three dimensionality.

Fig. 9 shows cavity mid-plane isotherms, notice that isotherms are irregular only near the walls due to the boundary layers. The temperature horizontal gradient is significantly large near the isothermal walls and minimal in the cavity center. The central area show negligible temperature gradients due to stratified region covers around 75% of the cavity length. On the other hand, in the region which the temperature horizontal gradient change locally of sign, is where secondary flow occurs.

4.2 Experimental Results

In this section we show a comparison between the Nusselt number and temperature profiles obtained from simulations and experiment. The Nusselt number is a dimensionless number defined as follows,

$$Nu_L = \frac{hL}{k_f} = \frac{\dot{q}L}{Ak_f(T_h - T_c)}, \quad (18)$$

where h is the convective heat transfer coefficient, L is the geometry characteristic length, k_f is

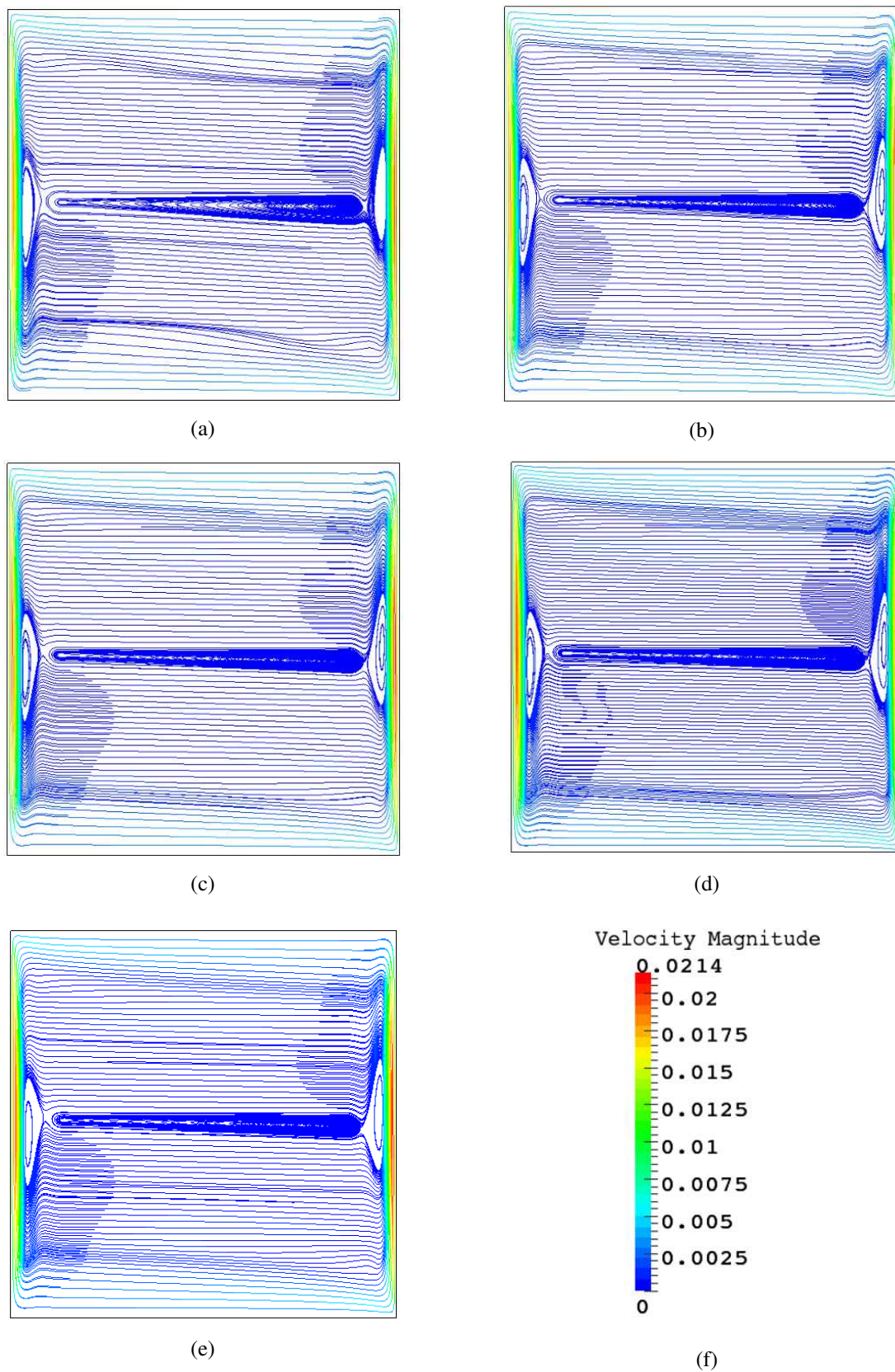


Figure 6: Streamlines at different vertical planes of the cavity at $Ra = 1.7 \times 10^8$ with variable viscosity. (a) $y = 0.1$, (b) $y = 0.2$, (c) $y = 0.3$, (d) $y = 0.4$, (e) $y = 0.5$, (f) Dimensionless velocity Magnitude Scale. The streamlines are colored with the velocity magnitude.

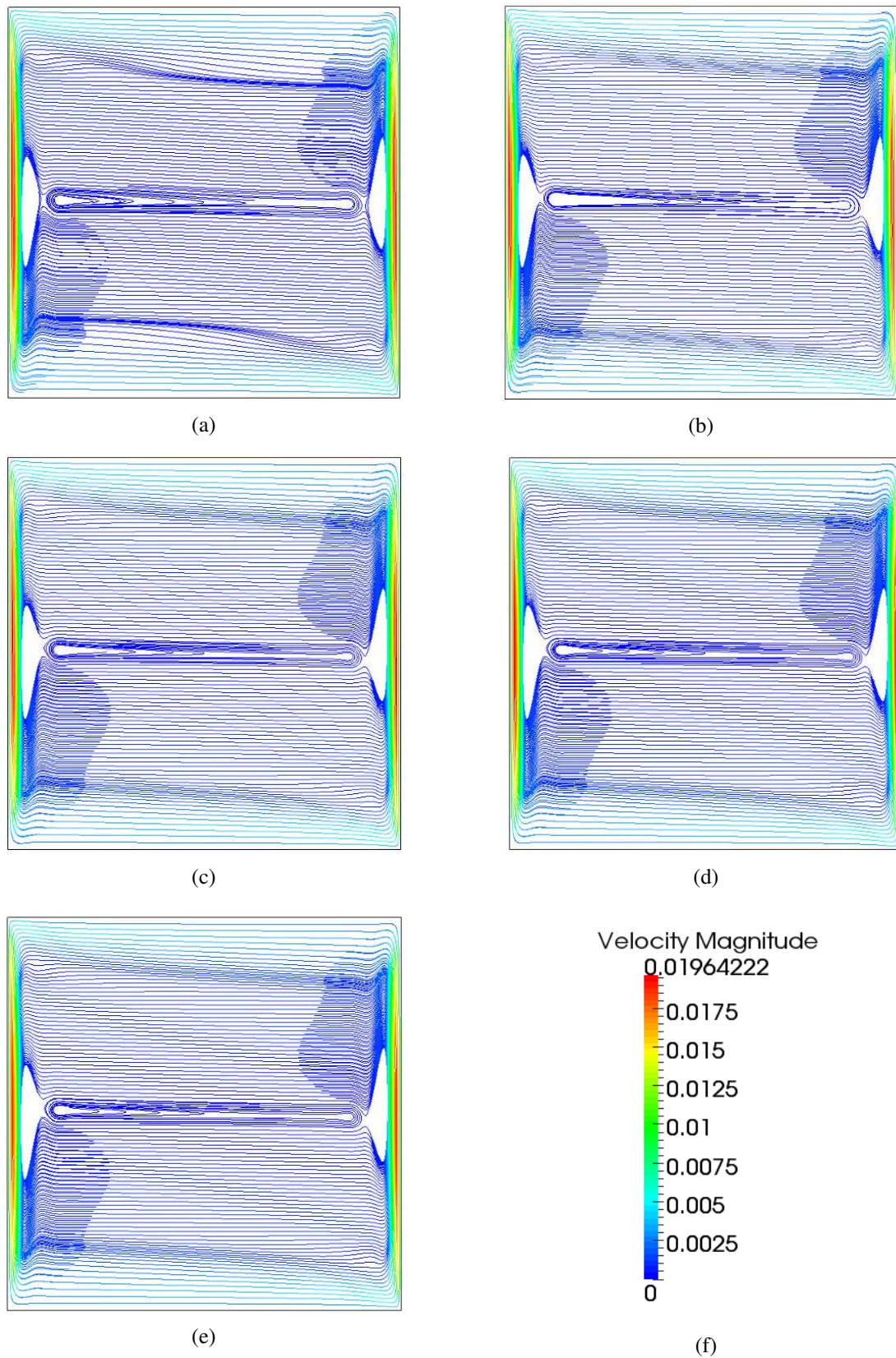


Figure 7: Streamlines at different vertical planes of the cavity at $Ra = 1.7 \times 10^8$ with constant viscosity. (a) $y = 0.1$, (b) $y = 0.2$, (c) $y = 0.3$, (d) $y = 0.4$, (e) $y = 0.5$, (f) Dimensionless velocity Magnitude Scale. The streamlines are colored with the velocity magnitude.

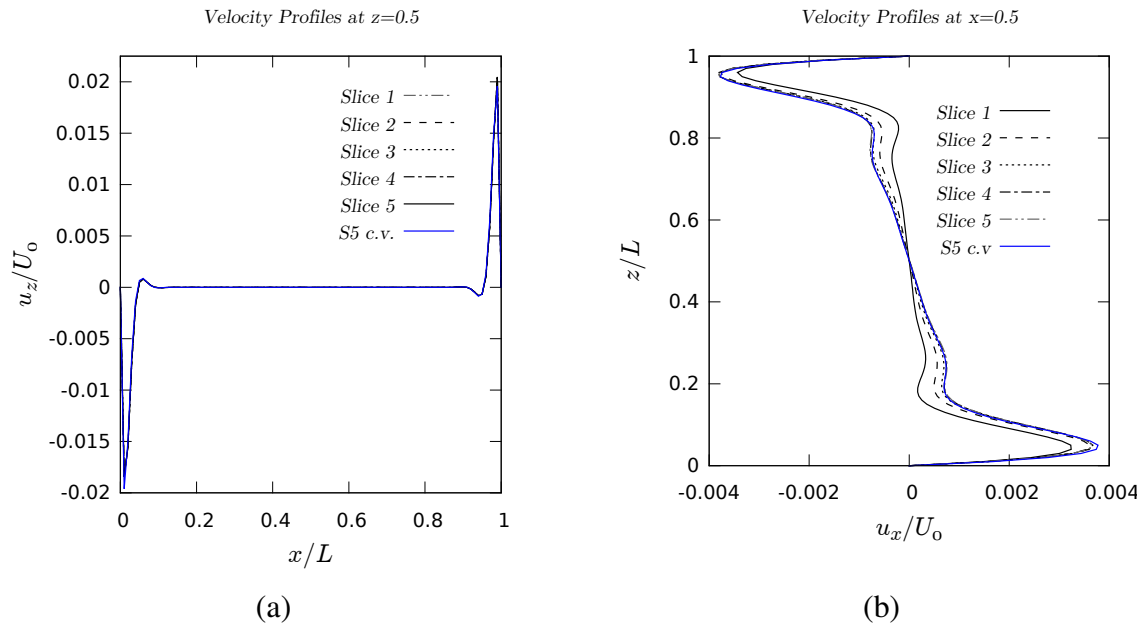


Figure 8: Velocity profiles at different heights of the cavity. (a) Horizontal Profile, (b) Vertical Profile.

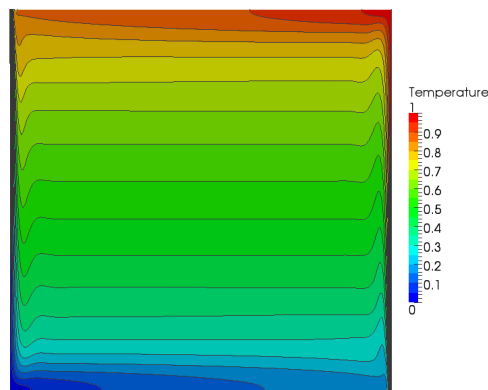


Figure 9: Isotherm at mid-plane of the cavity. The temperature is presented in a dimensionless form $(T - T_c)/(T_h - T_c)$.

	\overline{Nu}	u_x/U_0 ($x = 0.5$)	z/L ($x = 0.5$)	u_z/U_0 ($z = 0.5$)	x/L ($z = 0.5$)
Variable Viscosity (Numerical)	(hw) 36.2675	-0.00380	0.955	0.0204	0.990
	(cw) 36.1995	0.00367	0.050	-0.0184	0.010
Constant Viscosity (Numerical)	(hw) 36.0596	-0.00378	0.950	0.0196	0.990
	(cw) 36.0794	0.00378	0.050	-0.0196	0.010
Experiment	45.44 ± 6.07	--	--	--	--

Table 3: Comparison of Nusselt number and vertical and horizontal profiles peak values among the two numerical cases and the experiment at $Ra = 1.7 \times 10^8$.

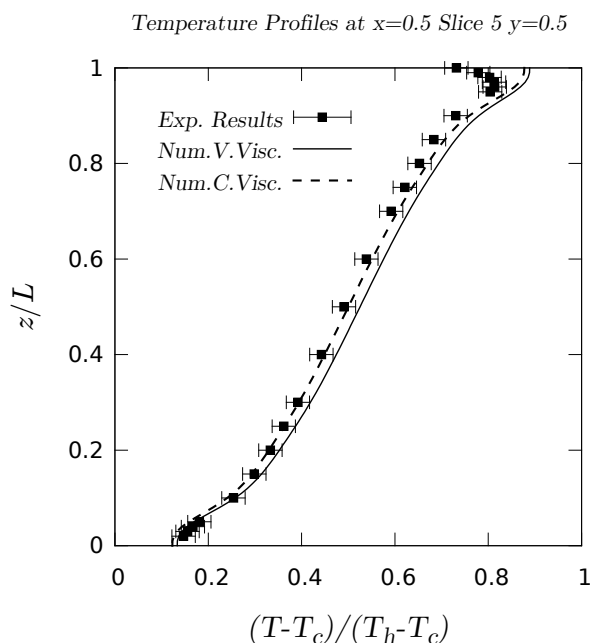


Figure 10: Comparison of vertical temperature profiles at mid-plane of the cavity between experimental and numerical results

the fluid thermal conductivity, \dot{q} is the total heat transferred to the system and A is the surface area. This number is related to the energy transferred by convection with respect to the energy transported by conduction. Numerically, the mean Nusselt is calculated by the expression (19). Experimentally, this dimensionless number is calculated by the expression (18) using the power measured value $\dot{q}_{avg} = (V_{rms})^2/R$, where V_{rms} is the heater analog voltage input and R is the heater resistance. These measured and calculated (in both cases: variable and constant viscosity) Nusselt values along with the vertical and horizontal profiles peak values are registered in table 3.

$$\overline{Nu}_L = \frac{L}{T_h - T_c} \left(\frac{1}{A} \int_{W_{all}} \frac{\partial T}{\partial x} d\Gamma \right). \quad (19)$$

As can be seen in Table 3, there is a difference between the calculated Nusselt number and the obtained from the power measurement, the difference is approximately 20% with respect to the measured value. This discrepancy may be caused by heat losses in the insulation system that can not be predicted by the mathematical model which considers idealized adiabatic boundary conditions at top, bottom and end walls. In fact, non-idealized thermal boundary conditions have been studied by Fusegi and Hyun (1994). They analyzed the discrepancies main causes between the available experimental and numerical predictions with idealized boundary conditions in a square cavity differentially heated. They remark that more realistic results can be obtained if one considers the thermal conductivity of the insulated wall. They show evidence, from other authors, of differences between the calculated Nusselt numbers with and without an alternative model for thermal boundary conditions in insulated walls.

In spite of the difference observed in table 3, between the numerical and experimental Nusselt values, there is a reasonable agreement among the calculated and measured temperature profiles. The Fig. 10 shows the temperature profiles along the central z -axis located at mid-plane of the

cavity. There is good agreement between the measurements and the numerical solution. The most pronounced difference is observed in the profile upper region. In the simulation, the top wall is ideally adiabatic, however in the experiment the profile upper region is affected by the opening used to introduce the temperature sensor.

On the other hand, the Nusselt number, in the constant viscosity case, is lower than in the temperature-dependent viscosity case. In this sense, these results coincide with those obtained by Hyun and Lee (1988) and Yamasaki and Thomas F. Irvine (1984). They suggest that viscosity temperature-dependence enhances the heat transfer. However, the difference in the heat transfer rates, in both cases is only about 0.45%, moreover, the temperature profile, using a mean value viscosity, has an excellent agreement with the experimental data. Despite this good approximation, the asymmetry of the velocity field observed in the first case, is not captured by the second case as can be shown in table 3 and also in the streamlines of the Figs. 6 and 7.

5 CONCLUSIONS

The present numerical study provides the basic flow patterns and heat transfer characteristics for natural convection in a cubical cavity with variable viscosity at $Ra = 1.7 \times 10^8$ with a reasonable agreement with the experimental data. Numerical predictions in the studied benchmark, using a mean constant value for the viscosity instead of a variable temperature-dependent function, are in accordance with the experimental results. However, using the potential law (15), it is possible to capture asymmetries of the flow pattern. The viscosity temperature-dependence causes a notable asymmetry in the velocity field and a flow concentration near the hot wall, also a slight heat transfer rate increment in the cavity. It would be interesting to include more realistic boundary conditions in the numerical model for further investigations and also improve the experimental setup to take account the principal heat losses.

ACKNOWLEDGMENT

We are grateful to Dr. Liliana Mogni, Member of the Materials Characterization Group of the Bariloche Atomic Center, for the collaboration and support on the viscosity measurements.

REFERENCES

- Arpaci V.S. Microscales of turbulence and heat transfer correlations. *International Journal of Heat and Mass Transfer*, 29:1071–1078, 1986.
- Arpino F., Massarotti N., and Mauro A. High rayleigh number laminar-free convection in cavities: New benchmark solutions. *Numerical Heat Transfer, Part B: Fundamentals*, 58(2):73–97, 2010.
- Bennett B.A.V. and Hsueh J. Natural convection in a cubic cavity: Implicit numerical solution of two benchmark problems. *Numerical Heat Transfer, Part A: Applications*, 50(2):99–123, 2006.
- Buchberg H., Catton I., and Edwards D.K. Natural convection in enclosed spaces—a review of application to solar energy collection. *Journal of Heat Transfer*, 98(2):182–188, 1976.
- Chenoweth D.R. and Paolucci S. Natural convection in a enclosed vertical air layer with large horizontal temperature differences. *Journal of Fluid Mechanics*, 169:173–210, 1986.
- Codina R. *A Finite Element Model for Incompressible Flow Problems*. Ph.D. thesis, 1992.
- Codina R. Comparison of some finite element methods for solving the diffusion-convection-reaction equation. *Computer Methods in Applied Mechanics and Engineering*, 156(1–4):185–210, 1998.

- De Vahl Davis G. Natural convection of air in a square cavity: A bench mark numerical solution. *International Journal for Numerical Methods in Fluids*, 3:249–264, 1983.
- Fusegi T., Hyun J., Kuwahara K., and Farouk B. A numerical study of three-dimensional natural convection in a differentially heated cubical enclosure. *International Journal of Heat and Mass Transfer*, 34(6):1543–1557, 1991.
- Fusegi T. and Hyun J.M. Laminar and transitional natural convection in an enclosure with complex and realistic conditions. *International Journal of Heat and Fluid Flow*, 15(4):258 – 268, 1994.
- Gastelurrutia J., Ramos J.C., and Larraona G.S. Numerical modelling of natural convection of oil inside distribution transformers. *Applied Thermal Engineering*, 31(4):493–505, 2011.
- Hiller W., Koch S., and Kowalewski T. Three-dimensional structures in laminar natural convection in a cubic enclosure. *Experimental Thermal and Fluid Science*, 2(1):34–44, 1989.
- Hyun J.M. and Lee J.W. Transient natural convection in a square cavity of a fluid with temperature-dependent viscosity. *International Journal of Heat and Fluid Flow*, 9(3):278 – 285, 1988.
- Janssen R., Henkes R., and Hoogendoorn C. Transition to time-periodicity of a natural-convection flow in a 3d differentially heated cavity. *International Journal of Heat and Mass Transfer*, 36(11):2927 – 2940, 1993.
- Leong W., Hollands K., and Brunger A. Experimental nusselt numbers for a cubical-cavity benchmark problem in natural convection. *International Journal of Heat and Mass Transfer*, 42(11):1979–1989, 1998a.
- Leong W., Hollands K., and Brunger A. On a physically-realizable benchmark problem in internal natural convection. *International Journal of Heat and Mass Transfer*, 41(23):3817–3828, 1998b.
- Lew A. *El método de elementos finitos en entornos de alta performance*. Master's Thesis, 1998.
- Mallinson G.D. and Davis G.D.V. Three-dimensional natural convection in a box: a numerical study. *Journal of Fluid Mechanics*, 83:1–31, 1977.
- Mamun M., Leong W., Hollands K., and Johnson D. Cubical-cavity natural-convection benchmark experiments: an extension. *International Journal of Heat and Mass Transfer*, 46(19):3655 – 3660, 2003.
- Paolucci S. and Chenoweth D.R. Transition to chaos in a differentially heated vertical cavity. *Journal of Fluid Mechanics*, 201:379–410, 1989.
- Peng Y., Shu C., and Chew Y.T. A 3d incompressible thermal lattice boltzmann model and its application to simulate natural convection in a cubic cavity. *J. Comput. Phys.*, 193(1):260–274, 2004.
- Pepper D.W. and Hollands K.G.T. Summary of benchmark numerical studies for 3-d natural convection in an air-filled enclosure. *Numer. Heat Transfer A*, 42:1, 2002.
- Tric E., Labrosse G., and Betrouni M. A first incursion into the 3d structure of natural convection of air in a differentially heated cubic cavity, from accurate numerical solutions. *International Journal of Heat and Mass Transfer*, 43(21):4043–4056, 2000.
- Wakashima S. and Saitoh T.S. Benchmark solutions for natural convection in a cubic cavity using the high-order time–space method. *International Journal of Heat and Mass Transfer*, 47(4):853 – 864, 2004.
- Yamasaki T. and Thomas F. Irvine J. Laminar free convection in a vertical tube with temperature-dependent viscosity. *International Journal of Heat and Mass Transfer*, 27(9):1613 – 1621, 1984.